The ArMexo - A upper-limb assistive rehabilitation system with a control approach based on a sliding modes*

Luis Leduc-Sahagun[1], Mariana Ballesteros[1], *Member, IEEE*, David Cruz-Ortiz[2], *Member, IEEE*

***Abstract*— This work presents the development of the ArMexo, an upper limb assistive rehabilitation system with four degrees of freedom (DoF) to assist the user in wrist radial/ulnar deviation, flexion/extension, pronation/supination, and elbow flexion/extension movements. The ArMexo is a self-designed exoskeleton manufactured mainly using a tridimensional printing system with polylactic acid (PLA) as the primary manufacturing material. As part of the actuation system, the proposed device considers four brushless motors model AK-60 of CubeMars coupled to a microcontroller Launchpad F28379xD of Texas Instruments™, where a first-order sliding mode (FOSM) serves as the control algorithm to regulate the trajectory tracking of each DoF of the ArMexo. A proportional-derivative (PD) controller was also implemented as part of the obtained results to prove the proposed FOSM's superior performance. Then, the experimental results show that the proposed controller guaranteed the trajectory tracking of reference trajectories with an error norm of less than six degrees.**

***Index Terms*— Upper limb, assistive rehabilitation exoskeleton, sliding modes.**

I. Introduction

In 2023, the National Institute of Statistics and Geography (INEGI) of Mexico reported that 8.9 million Mexicans have a disability. This equates to 6.8% of the country's population with a disability condition, a higher rate than the reported in 2018, which was 6.3%. In this sense, the age groups most affected by disabilities are those aged 60 and over (49.4% of the population) and those aged 30-59 (34.2% of the population). Furthermore, the INEGI report indicated that 12.3% of individuals with disabilities encounter difficulties in performing activities such as bathing, dressing, and eating. Additionally, 17.2% of this population group faces challenges in moving or using their arms or hands in their activities of daily living (ADLs) [1].

In that sense, it is well-known that rehabilitation therapy increases the quality of life in people with disabilities. However, conventional therapies imply a time-consuming and arduous process depending on the availability of resources, the capacity of medical personnel, and the provision of adequate patient care [2]. The limitation of conventional therapy and the high demand for this service have encouraged the development and introduction of novel and more efficient rehabilitation approaches, including the implementation of robotic systems, which, according to recent studies, facilitate intensive, precise, quantitative, and safe rehabilitation [3].

Conventionally, rehabilitation robots are programmed to compute the required torque to regulate movements in each joint of the limbs [4], [5]. Therefore, it is essential to implement control algorithms to ensure that the desired trajectories are followed.

In that sense, position control strategies are commonly used in rehabilitation robots to move their joints at a desired angle and consequently, the user limbs according to a set of reference trajectories [6]; one of these control techniques is the proportional derivative controller (PD), which mainly reacts to position and velocity errors and does not require system identification. However, the gain-tuning can be highly time-consuming since an inadequate adjustment can produce large torques, which may damage the actuators and the patient [7], [8]. Moreover, this control scheme is not the best option for dealing with nonlinear dynamics in the system aside from external perturbations.

Other control algorithms used in rehabilitation robots are: impedance control aims to have the position and velocity errors follow desired trajectories performed by human interactions, which allows stable interactions between exoskeletons and patients in stiff environments. However, the precision and accuracy of this class of control algorithms are compromised since this control scheme can be unstable when the impedance is high [9], [8].

Admittance control is another option to solve the trajectory tracking problem of robotic rehabilitation systems because this control allows smooth movements. Nevertheless, these control algorithms may give the user a non-realistic sensation [10]. Consequently, this strategy requires high transmission ratios to achieve precise motion, and a high admittance can destabilize the system [8]. Particularly, these algorithms require a model-based control to establish a dynamic relationship between the system's motion and the human-robot interactions, which is challenging to implement in systems with complex geometries.

On the other hand, adaptive controllers are able to adjust the system's unknown variances since the controller parameters are updated based on the difference between the values measured by the system's sensors and those from a reference model, which allows compensation for modeling uncertainties. However, these methods cannot handle external disturbances in the system and fast-changing parameters [8].

*This work was supported in part by the Instituto Politécnico Nacional, under Grants: SIP-20250223, and SIP-20250253. The authors thank the support provided by Secretaria de Educacion, Ciencia, Tecnologia e Innovacion de la Ciudad de Mexico (SECTEI) under the grant SECTEI/081/2024. Luis Leduc-Sahagun is sponsored by a Mexican scholarship from the SECIHTI, CVU: 2062702.

[1] Medical Robotics and Biosignals Lab, CIDETEC, Instituto Politécnico Nacional, Gustavo A. Madero, Mexico City. email: lleducs1400@alumno.ipn.mx, mballesterose@ipn.mx.

[2] Medical Robotics and Biosignals Lab, UPIBI, Instituto Politécnico Nacional, Av. Acueducto S/N, La Laguna Ticoman, Gustavo A. Madero, 07340, Mexico City, Mexico. email: dcruzo@ipn.mx.

As a remarkable solution, sliding mode controllers (SMC) have demonstrated resilience and stability in the presence of parametric uncertainties and system disturbances. In addition, a sliding surface made up of a combination of error signals is adopted, and the tracking error is reduced to a certain acceptable level [11]. Various techniques for making SMC adaptive have been proposed, including the use of the boundary layer method, the incorporation of a proportional-integral-derivative (PID) controller, the application of fuzzy logic, the integration of a nonlinear disturbance observer, the implementation of baseline SMC, the adoption of terminal, and the use of fast terminal SMC [12].

Based on the above arguments, this paper presents the development of an upper-limb assistive rehabilitation system (ULARS) called ArMexo. The main contributions of this work are:

- A self-design of a ULARS of four DoF considering Mexican adults' anthropometric dimensions.
- The implementation of a first-order sliding mode (FOSM) control to guarantee the trajectory tracking of the ArMexo.

II. Biomechatronic System Description

The proposed device considers as part of its mechanical structure four degrees of freedom (DoF), which correspond to the movements of flexion/extension of the elbow (FEE), radial/ulnar deviation of the wrist (RUD), flexion/extension of the wrist (FEW), and pronation/supination of the wrist (PSW). The previous movements were considered since, according to the literature, these DoF are the most relevant in executing the ADLs. The ranges of motion (ROM), aside from the speeds and torque required to execute the human ADLs, were consulted from [13], [14] and [15], respectively.

On the other hand, the anthropometric dimensions of 203 men and 278 women between 18 and 64 years from the Mexican population were analyzed to define the dimensions of the ArMexo. The measures considered included the length of the forearm, the length of the hand, the width of the hand, and the height from the ground to the knee [16]. Table I summarizes the measures considered in this work, such as the torque and speed of the actuators used.

Once the anthropometric measures were analyzed, the main dimensions of the system were defined. Figure 1 shows an isometric view of ArMexo, showing A) the segment of the aluminum base used to carry the ULARS, B) the length of the forearm, which has adjustable dimensions from 25.8 to 28.8 cm, C) the hand width, which corresponds to a fixed dimension, D) the hand length, which can be adjusted according to the user's needs from 7.2 to 12 cm, and finally E) the ground to knee height, which, like segments B) and D), is also an adjustable segment from 71 to 76 cm. These dimensions are shown in Table I.

A. Kinematics of the exoskeleton

Since the ArMexo considers four DoF in its mechanical structure, Figure 2 shows a general scheme to evidence the user collocation in the system. Particularly, Figure 2-A), shows the distribution of each DoF; in orange is shown the rotation axis of FEE, this DoF will now be denoted by γ; in orange, the axis of PSW in red, described by δ. The axis of RUD is shown in yellow with β, whereas FEW is in green, represented by α. In Figure 2-B), the CAD model of ArMexo is shown, where the wrist joints are aligned on a blue marker, and the FEE joint is aligned with the user's joint. It is important to mention that the incidence angle in the upper limb was considered when designing the exoskeleton, which is 12.5 degrees since the average of 11 degrees in men and 14 degrees in women was taken [17].

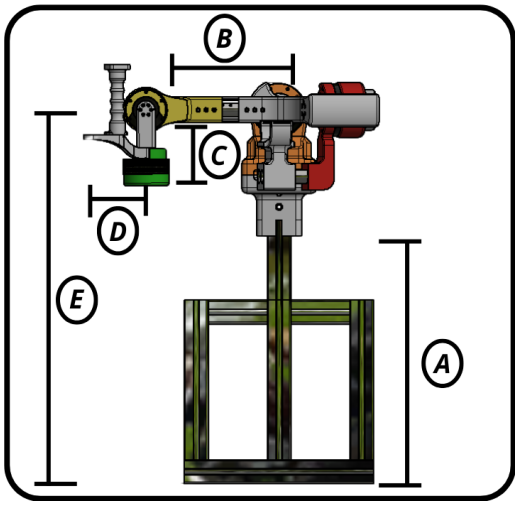

Fig. 1. Main segments of the ArMexo system.

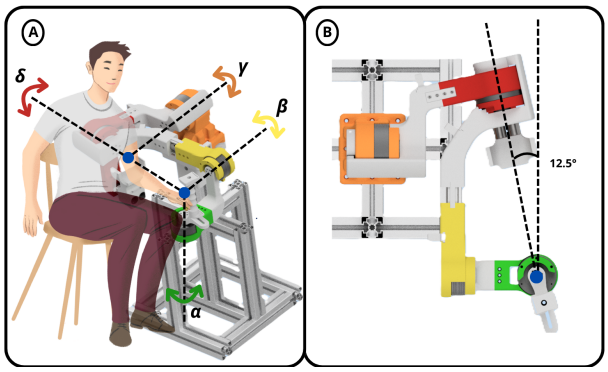

Fig. 2. Mechanical structure of the ArMexo system, A) System configuration, B) CAD model.

B. Manufacture of the system

The parts integrating this device were manufactured using three-dimensional printing techniques with polylactic acid (PLA) as primary material with a filler of 70%. In addition, a carbon fiber tubular segment was used in the adjustable forearm segment, as well as in the internal part of the joint between the FEE-PSW segment and two more segments for the elbow-forearm support. The base that supports the whole system was machined using aluminum profiles of 4.5×4.5 cm. The materials used for this device were considered due

TABLE I

MEXICAN POPULATION DIMENSIONS AND THOSE USED BY ARMEXO. BIOMECHANICAL DATA OF HUMAN ELBOW AND WRIST AND THOSE CONSIDERED FOR ARMEXO.

		Human			ArMexo		
Dimensions	Ground to knee height	71.7 cm			71 - 76 cm		
	Forearm length	23.5 cm			25.8 - 28.8 cm		
	Hand length	17.1 cm			7.2 - 12 cm		
	Hand width	9.3 cm			9.6 cm		
		ROM	**Velocity**	**Torque**	**ROM**	**Velocity**	**Torque**
Flexion/extension of the elbow (FEE)		140° / 0°	173 deg/s	17.5 Nm	60° / 0°	3618 deg/s	12 Nm
pronation/supination of the wrist (PSW)		100° / 100°	489 deg/s	15.3 Nm	25° / 25°	3618 deg/s	12 Nm
Radial/ulnar deviation of the wrist (RUD)		35° / 35°	204 deg/s	10.4 Nm	35° / 35°	1398 deg/s	9 Nm
Flexion/extension of the wrist (FEW)		85° / 85°	233 deg/s	8.5 Nm	60° / 60°	1398 deg/s	9 Nm

to their mechanical properties [18]. The wiring for each of the actuators was attached to the back of each of the joints, where the structural design passes the wiring through, avoiding direct contact with the user.

C. Actuation system and microcontroller

The electronic instrumentation of the system considers the use of four CubeMars brushless motors, using a 24 V, 40 A supply to power each motor. The integrated controller board for each motor includes a 14-bit absolute encoder, which allows the angular position of each actuator to be received with a resolution of 0.1 degrees, as well as the speed, torque, and temperature of each actuator. Notably, for FEE and PSW, motors model AK-80-6 are used, which, as shown in Table I, are capable of providing a torque of 12 Nm, with a speed of 3618 deg/s, whereas for RUD and FEW, motors model AK-60-6 were used, which provide 9 Nm of torque and a speed of 1398 deg/s [19], [20]. The motor's output torque and design make these actuators suitable for the device, as they can be aligned directly to each joint without needing additional transmission systems.

This study uses the CAN communication protocol to receive and send information from each actuator to the microcontroller. The microcontroller is the intermediary between the host computer and the receiving and sending of data. The microcontroller is the Texas Instruments LAUNCHXL-F28379D, a dual-core design with a 32-bit processing capability and a CAN module for real-time control applications, as it supports speeds of up to 1 Mbit/s. The microcontroller is a dual-core design with a 32-bit processing capability and a CAN module for real-time control applications. A FOSM algorithm is embedded in the microcontroller for each of the actuators. This FOSM control regulates the current value sent to the motor to obtain the desired torque to perform the mobilization in each DoF. Likewise, the serial communication port is used to communicate between the host computer and the microcontroller at a speed of 460800 baud.

D. System integration

Once all the elements comprising the ArMexo system were established, the next step consisted of integrating the device. Figure 3 shows the distribution of the four DoF in the system denoted by α, β, γ, and δ, respectively. Here, it is important to notice that each joint in the ArMexo has mechanical stops that delimit the ROM to guarantee the user's safety.

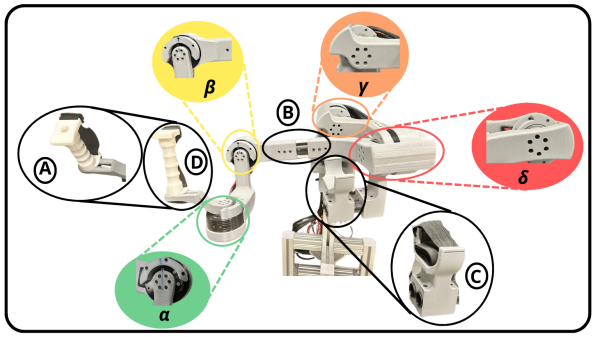

Fig. 3. Integration of the ArMexo system, A) Adjustable hand length, B) Adjustable forearm segment, C) Elbow support, D) Handle.

The proposed system considers its mechanical structure elements, allowing it to adjust for users with different anthropometric dimensions. Here, the distance between device joints ensures that the user can naturally perform wrist, forearm, and elbow movements throughout their ROM without collisions. Figure 3 evidenced the leading segments in the device where A) shows the adjustable hand length segment, while B) shows the adjustable forearm length segment. The adjustable dimensions considered for the system are summarized in Table I, where it can be observed that the height of the exoskeleton, the length of the forearm segment, aside from the length of the hand, can be modified.

In addition, the designed system has elbow support (See Figure 3 C)) to improve its use by the user. Notice that the designed support allows the correct alignment of the FEE and PSW joints, as well as an attachment for those users who are not able to maintain a posture for prolonged periods during rehabilitation sessions and avoid compensatory movements; this support also has a band that can be easily adjusted to the user's forearm.

Finally, Figure 3 D) shows a handle for the user to hold the device. The handle allows the correct alignment of the wrist with the joints of the ArMexo. If the user cannot grip the handle, it has a band to keep the user's hand in that position.

E. User interface

Regarding the software, two codes were used to operate the ArMexo system. The first code was programmed using Simulink from Matlab®, which is then embedded in the

microcontroller using the C2000 Processors toolbox. On the other hand, there is a Graphical User Interface (GUI), also developed in Simulink, where the system operator can monitor the performance of the exoskeleton. In the GUI, the signals obtained from each actuator can be displayed simultaneously, showing position, velocity, and torque. At the same time, this interface triggers and stops the actuators' operation, allowing the tuning of the gains for the control algorithms that can be implemented. This interface also has a button to set the user's initial points, as well as another button to return the device to the user's initial points.

III. Control Strategy

Consider the ArMexo system the vector $\mu \in \mathbb{R}^4$ defined as $\mu = \{\alpha, \beta, \gamma, \delta\}$ denotes the position vector of the system. Then, let introduce the state variables $x_1 \in \mathbb{R}^4$ and $x_2 \in \mathbb{R}^4$. with $x_1 = \mu$ and $x_2 = \dot{\mu}$.

Following the methodology proposed in [21], and taking into account that each DoF of ArMexo is actuated independently, each joint can be described in general form by the following second-order differential equation.

$$\begin{aligned} \dot{x}_{1,j}(t) &= x_{2,j}(t), \\ \dot{x}_{2,j}(t) &= f_j(X,t) + g_j(x_1,t)\tau_j(t) + \chi_j(X,t), \end{aligned} \tag{1}$$

where the state vector of the system is given by $X = \begin{bmatrix} x_1^\top & x_2^\top \end{bmatrix}^\top$. The output of the system is denoted by $y_j \in \mathbb{R}^2$, which satisfy $y_j = \begin{bmatrix} x_{1,j} & x_{2,j} \end{bmatrix}^\top$, $j = \{1,2,3,4\}$. In the equation (1), the nonlinear function $f_j : \mathbb{R}^8 \times \mathbb{R}^+ \to \mathbb{R}$ denotes the drift term of the exoskeleton, which is an unknown but is assumed locally Lipschitz, $g_j : \mathbb{R}^4 \times \mathbb{R}^+ \to \mathbb{R}$ is the input associated function assumed invertible $\forall t \in \mathbb{R}^+$, $\tau_j : \mathbb{R}^+ \to \mathbb{R}$ denotes the control signal for the j-th DoF of the ArMexo, whereas the nonlinear function $\chi_j : \mathbb{R}^8 \times \mathbb{R}^+ \to \mathbb{R}$ represents the internal uncertainties and external bounded perturbations affecting the system.

A. Problem statement

In this study, the control problem can be defined in terms of solving the trajectory tracking between the states of the ArmMexo given by $x_{1,j}$ and the corresponding reference trajectory $x_{1,j}^*$ despite the external perturbations. Here, the desired trajectory is assumed to be a smooth function designed as a sum of sigmoidal functions according to the methodology proposed in [22]. Then, let us define the tracking error as $e = \begin{bmatrix} e_{1,j} & e_{2,j} \end{bmatrix}^\top$, where

$$\begin{aligned} e_{1,j}(t) &= x_{1,j}(t) - x_{1,j}^*(t), \\ e_{2,j}(t) &= x_{2,j}(t) - x_{2,j}^*(t). \end{aligned} \tag{2}$$

Here, the derivative of the reference is denoted by $x_{2,j}^*$. The full-time derivative of (2) satisfy that

$$\begin{aligned} \dot{e}_{1,j}(t) &= e_{2,j}(t), \\ \dot{e}_{2,j}(t) &= f_j(X,t) + g_j(x_1,t)\tau_j(t) + \chi_j(X,t) - \dot{x}_{2,j}^*(t). \end{aligned} \tag{3}$$

Then, the problem statement can be rewriting as

$$\lim_{t\to\infty} \|e_{1,j}(t)\| = 0, \quad \forall t \geq 0, \tag{4}$$

Now, following the methodology proposed in [23], let introduce the control law τ_j defining a FOSM control algorithm, satisfying

$$\tau_j(t) = -\lambda_j \text{sign}(s_j(t)), \tag{5}$$

where $\lambda_j \in \mathbb{R}^+ \backslash \{0\}$ denotes the control gain, whereas $s_j \in \mathbb{R}$ represent the sliding surface, which satisfy

$$s_j(t) = e_{1,j}(t) + \rho_j e_{2,j}(t), \tag{6}$$

with $\rho_j \in \mathbb{R}^+$ chosen as a positive constant greater than zero that characterizes the convergence of the tracking error.

IV. Experimental results

As part of the control algorithm implementation, Figure 4 illustrates a flowchart that describes the system's general workflow, connections, and data sending and receiving between each component.

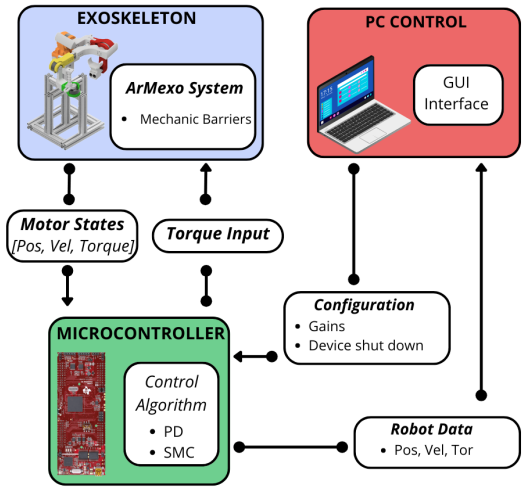

Fig. 4. Workflow of the stages considered in the ArMexo functioning.

Then, according to Figure 4, the system operator runs the GUI on the host computer, where it starts receiving the system status passing through the microcontroller. As mentioned before, the microcontroller has embedded the control algorithm, which allows it to compute the output torque necessary to mobilize the device. Here, the torque computation depends on two main parameters: the gains sent through the GUI and the current states of each actuator. Meanwhile, these states of each motor and the calculated torque are sent through the CAN communication protocol, where two-way communication is maintained through a serial communication protocol with the host computer. Also, in this section, the operator can monitor the current position, velocity, and torque while the user is in each wrist and elbow joint session, while man-machine interaction occurs.

Two control schemes have been implemented to compare the obtained performance as part of the experimental results: a FOSM and a conventional PD controller. Then, to achieve

the correct control implementation, the position and velocity of each actuator are required. In this case, both signals are provided by the actuation system; nevertheless, the velocity is computed with an Euler derivative, and the noise in the signal is evident. With this in mind, the control implementation considers a finite-time differentiator called the Super-Twisting Algorithm (STA) to compute the time derivative of the tracking error [24].

A. Control implementation

As previously mentioned, each reference trajectory was designed as a sum of four sigmoidal functions following the methodology proposed in [22]. However, it is not limited to other trajectories. These must be smooth, continuous, and at least twice differentiable. The ROMs given in Table I were considered here. Then, each reference trajectory starts at 0 degrees; the first sigmoid reaches the maximum positive value, the second sigmoidal is used to return to 0 degrees, the third one goes from zero to the maximum negative value, and the last one returns to zero. The sum of these four sigmoids has a duration of 11.75 seconds. For this work, this signal was repeated four times (See Figure 5).

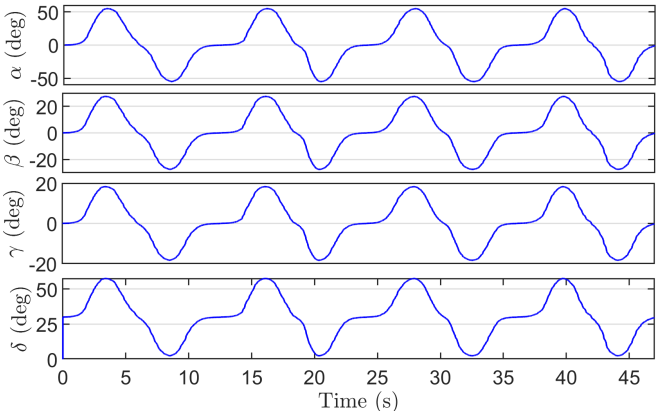

Fig. 5. Set of reference trajectories.

The frequency of the PD and FOSM control is 1600 Hz. The gains for both controls were selected experimentally. Figure 6 shows the trajectory tracking of joint α, with the performance of the PD controller in the first graph. Notice that the trajectory tracking presents deviations in t equal to 20, 30, and 43 seconds. On the other hand, the FOSM control performs better during the 47 seconds of the test. The same behavior occurs with β, γ, and δ, where the FOSM controller evidenced a superior performance. See Figures 7, 8 and 9 respectively.

To summarize the performance obtained with both implemented controllers, Figure 10 shows the norm of the trajectory tracking error of both controllers, the PD controller in blue and the FOSM controller in green. Notice that the convergence of both controllers occurs in the first seconds of the test. However, the PD algorithm presents oscillations between 5 and 12 degrees, while the FOSM presents a peak of 7 degrees.

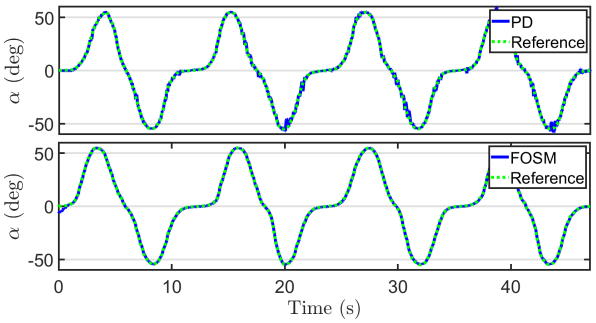

Fig. 6. Trajectory tracking performance of α.

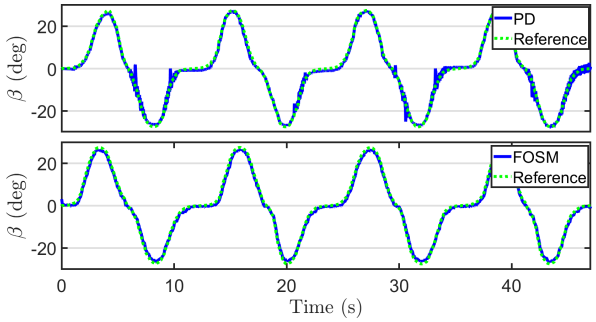

Fig. 7. Trajectory tracking performance of β.

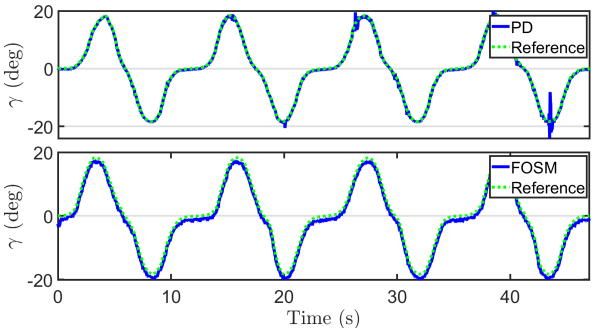

Fig. 8. Trajectory tracking performance of γ.

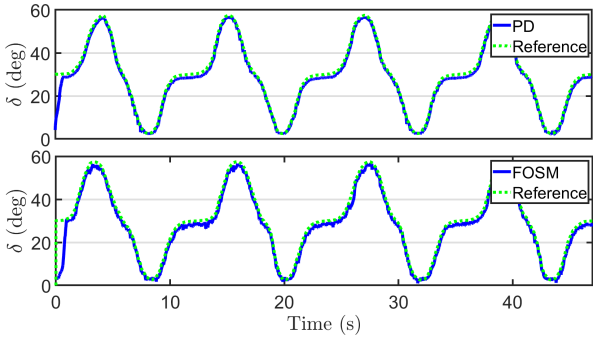

Fig. 9. Trajectory tracking performance of δ.

Finally, Figure 11 shows the integral of the norm of the control signals. This figure evidences that the FOSM's energy consumption is lower than that of the PD controller.

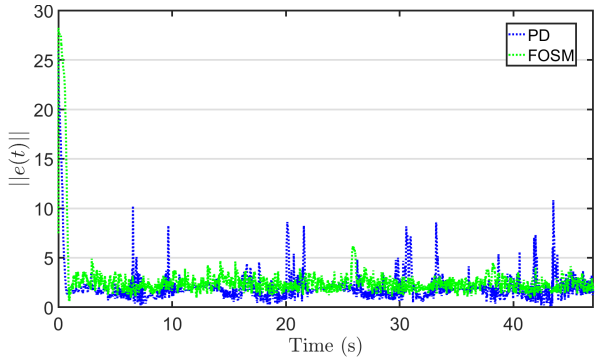

Fig. 10. Comparison of the error norm obtained with the PD and FOSM controllers.

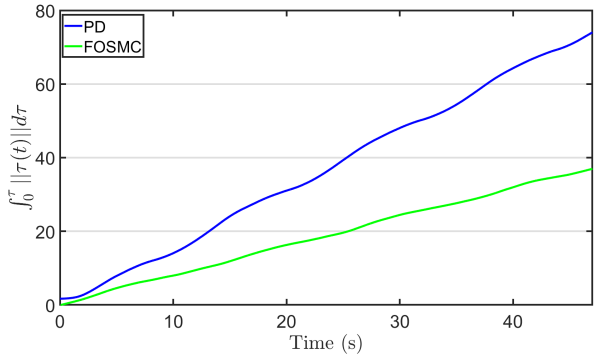

Fig. 11. Integral of the control signal norm.

V. Conclusions

In this work, a ULARS was designed according to the anthropometric dimensions of the Mexican adult population. As a result, a functional and adjustable device that allows the upper limb movements to execute the ADLs, considering the torque and ROM needed in adult users. The proposed control algorithm based on sliding modes solved the trajectory tracking problem. The results showed that the FOSM control guaranteed an error norm lower than the PD controller, since the maximum oscillation is 7 degrees against 12 degrees of the PD. The integral of the control norm depicted that the FOSM in the proposed setup required less energy than the PD controller.

The PD controller has significant oscillations in the trajectory tracking, which is reflected in the energy consumption, while the FOSM has a lower consumption. The FOSM controller guarantees trajectory tracking with the ROMs proposed at the beginning of this work in ULARS, which leads to the implementation of other types of trajectories according to the needs of Mexican patients.

References

[1] I. N. de Estadística y Geografía, "Encuesta nacional de la dinamica demografica (enadid) 2023," 2024.

[2] M. Righi, M. Magrini, C. Dolciotti, and D. Moroni, "A system for neuromotor based rehabilitation on a passive robotic aid," *Sensors*, vol. 21, no. 9, p. 3130, 2021.

[3] H. M. Qassim and W. Wan Hasan, "A review on upper limb rehabilitation robots," *Applied Sciences*, vol. 10, no. 19, p. 6976, 2020.

[4] R. Bogue, "Rehabilitation robots," *Industrial Robot: An International Journal*, vol. 45, no. 3, pp. 301–306, 2018.

[5] S. Głowiński and A. Błażejewski, "An exoskeleton arm optimal configuration determination using inverse kinematics and genetic algorithm," *Acta of bioengineering and biomechanics*, vol. 21, no. 1, 2019.

[6] W. Meng, Q. Liu, Z. Zhou, Q. Ai, B. Sheng, and S. S. Xie, "Recent development of mechanisms and control strategies for robot-assisted lower limb rehabilitation," *Mechatronics*, vol. 31, pp. 132–145, 2015.

[7] W. Yu, X. Li, and R. Carmona, "A novel pid tuning method for robot control," *Industrial Robot: An International Journal*, vol. 40, no. 6, pp. 574–582, 2013.

[8] G. Bauer and Y.-J. Pan, "Review of control methods for upper limb telerehabilitation with robotic exoskeletons," *Ieee Access*, vol. 8, pp. 203382–203397, 2020.

[9] R. Riener, L. Lunenburger, S. Jezernik, M. Anderschitz, G. Colombo, and V. Dietz, "Patient-cooperative strategies for robot-aided treadmill training: first experimental results," *IEEE transactions on neural systems and rehabilitation engineering*, vol. 13, no. 3, pp. 380–394, 2005.

[10] T. Proietti, V. Crocher, A. Roby-Brami, and N. Jarrasse, "Upper-limb robotic exoskeletons for neurorehabilitation: a review on control strategies," *IEEE reviews in biomedical engineering*, vol. 9, pp. 4–14, 2016.

[11] L. Teng, M. A. Gull, and S. Bai, "Pd-based fuzzy sliding mode control of a wheelchair exoskeleton robot," *IEEE/ASME Transactions on Mechatronics*, vol. 25, no. 5, pp. 2546–2555, 2020.

[12] S. F. Ahmed, Y. Raza, H. F. Mahdi, W. W. Muhamad, M. K. Joyo, A. Shah, and M. Koondhar, "Review on sliding mode controller and its modified types for rehabilitation robots," in *2019 IEEE 6th International Conference on Engineering Technologies and Applied Sciences (ICETAS)*, pp. 1–8, IEEE, 2019.

[13] M. Hillman, "2 rehabilitation robotics from past to present–a historical perspective," *Advances in rehabilitation robotics: human-friendly technologies on movement assistance and restoration for people with disabilities*, pp. 25–44, 2004.

[14] S. Hesse, C. Werner, M. Pohl, S. Rueckriem, J. Mehrholz, and M. Lingnau, "Computerized arm training improves the motor control of the severely affected arm after stroke: a single-blinded randomized trial in two centers," *Stroke*, vol. 36, no. 9, pp. 1960–1966, 2005.

[15] P. Boissy, D. Bourbonnais, D. Gravel, A. B. Arsenault, and M. Leblanc, "A static dynamometer measuring simultaneous torques exerted at the upper limb," *IEEE Transactions on Rehabilitation Engineering*, vol. 6, no. 3, pp. 309–315, 1998.

[16] R. Á. Chaurand, L. R. P. León, and E. L. G. Muñoz, *Dimensiones antropométricas de población latinoamericana*. Universidad de Guadalajara, CUAAD, 2007.

[17] D. M. Scarborough, R. C. McCunney, E. M. Berkson, and L. S. Oh, "The relationship of elbow alignment and kinematics on shoulder torque during the softball pitch: a biomechanical analysis of female softball pitchers," *Journal of Shoulder and Elbow Surgery*, vol. 28, no. 2, pp. 357–364, 2019.

[18] M. Jiang, Z. Zhou, and N. Gravish, "Flexoskeleton printing enables versatile fabrication of hybrid soft and rigid robots," *Soft robotics*, vol. 7, no. 6, pp. 770–778, 2020.

[19] CubeMars, "Ak80-6 ak series robotic actuation module."

[20] CubeMars, "Ak60-6 ak series robotic actuation module."

[21] D. Cruz-Ortiz, I. Chairez, and A. Poznyak, "Non-singular terminal sliding-mode control for a manipulator robot using a barrier lyapunov function," *ISA transactions*, vol. 121, pp. 268–283, 2022.

[22] D. Cruz-Ortiz, M. Ballesteros-Escamilla, I. Chairez, and A. Luviano, "Output second-order sliding-mode control for a gecko biomimetic climbing robot," *Journal of Bionic Engineering*, vol. 16, no. 4, pp. 633–646, 2019.

[23] R. Garcia-Leal, D. Cruz-Ortiz, M. Ballesteros, and J. C. Huegel, "Development of the biomech-wrist: A 3-dof exoskeleton for rehabilitation and training of human wrist," in *2023 International Conference on Rehabilitation Robotics (ICORR)*, pp. 1–6, IEEE, 2023.

[24] I. Salgado, I. Chairez, O. Camacho, and C. Yañez, "Super-twisting sliding mode differentiation for improving pd controllers performance of second order systems," *ISA transactions*, vol. 53, no. 4, pp. 1096–1106, 2014.